NUEJ
Naresuan University
Engineering Journal

Numerical heat transfer study of an impinging jet of nanofluid of TiO_2 on a chip surface

Koonlaya Kanokjaruvijit*, Kamolthip Tuamjan, Pimwipa Srirat, Taechinee Rattanasangsri, Suttinon Panyadibwong and Pongpun Othaganont

Department of Mechanical Engineering, Faculty of Engineering, Naresuan University, Phitsanulok, Thailand

* Corresponding author e-mail: koonlayak@nu.ac.th, koonlaya@gmail.com

(Received: 18 April 2022, revised: 29 August 2022, Accepted: 5 September 2022)

Abstract

A numerical investigation of 2D axisymmetric heat transfer of an impinging jet of water-based titanium dioxide (TiO_2) nanofluid on a CPU chip surface is performed by using the finite element method with k-ε turbulence model with the wall treatment. The flat plate impingement is also studied to compare the heat transfer and flow characteristics with those of the chip plate and the average heat transfer results agree well with the experimental results obtained from literature. Parametric effects such as nanofluid concentration (ϕ), Reynolds number (Re_{Dj}) and jet-to-plate spacing (H/D_j) are examined. The nanofluid concentration is in the range of 0-6% by volume. The tested Re_{Dj} is between 2000 and 8000. The jet-to-plate spacing is between 2-4. The maximum heat transfer enhancement in terms of average Nusselt number of the TiO_2 nanofluid compared to that of the water is 18.24% for the chip plate impingement at Re_{Dj} = 2000 and ϕ = 6%; however, this maximum enhancement is 47.13% in terms of the average heat transfer coefficient. After the multiple linear regression analysis, the nondimensional heat transfer correlations are obtained. Finally, the ratios of pumping power between nanofluid and base fluid are plotted and found the penalty of 1.5 to nearly 4 times.

Keywords: Jet Impingement, Nanofluid, Titanium Dioxide, CPU Chip

1. NOMENCLATURE

c_p	specific heat, J/kg-K
D_j	jet diameter, m
h	heat transfer coefficient, W/m^2-K
H	distance between jet exit and stagnation point, m
k	turbulent kinetic energy
Nu	Nusselt number
PP	pumping power, W
q_s''	surface heat flux, W/m^2
r	radial coordinate, m
R_{chip}	radius of chip, m
R_s	radius, m
Re_{Dj}	Reynolds number based on jet diameter
p	pressure, Pa
T	temperature, K
u	fluid velocity, m/s
z	axial coordinate, m

Greek symbols

ε	dissipation rate of turbulent kinetic energy
λ	thermal conductivity
μ	fluid dynamic viscosity, Pa-s
ϕ	nanoparticles volume fraction
ρ	density

Subscripts

avg	average property
bf	with respect to base fluid
chip	with respect to chip
j	with respect to jet
nf	with respect to nanofluid
p	with respect to nanoparticles
s	with respect to surface

2. INTRODUCTION

Due to the increasing need for shrinking the size of electronic components while enhancing their capacity, the heat fluxes or power density is then substantially increased. Conventional heat sink used as a passive cooling method has probably become unfit to the packaging of the devices. Direct heat transfer from each component has been brought to a few researchers' interests and proved that it is a promising cooling scheme design for the next-generation higher performance devices. van Erp et al. (2020) has proposed a new design of electronic cooling by directly embedding multiple microfluidic channels inside the chip substrate using water as working fluid and reported the heat removal of 17 kW/cm^2 with only 0.57 W/cm^2 pumping power. Direct multiple impinging jets on a high-power device was proposed by Wei et al. (2019) reporting the highest heat transfer coefficient of 6.25×10^4 W/m^2-K with the pumping power as low as 0.3 W.

Nanofluid jet impingement has recently attracted an increasing number of researchers since Choi and Eastman have discovered the enhancement of base fluid thermal conductivity by using nanoparticles in 1995. Thus, the nanofluid could become a game changer in the heat transfer augmentation for components that are exposed to a high heat generation such as heat exchangers, electronic components, automobile components and thermal treatment of metals. In addition to increasing the thermal conductivity of the base fluid, Lv et al. (2017a,b) explained how the nanofluid augmented heat transfer in a single free impinging jet by the fact that the nanoparticles vigorously bombarded at the impingement surface. This caused intense turbulence and thinner boundary layer thickness near the surface leading to the heat transfer improvement.

Generally, the base fluids of the nanofluids are water, engine oil and ethylene glycol. However, most studies have used water or deionized water. The nanoparticles are usually metallic compounds such as Al_2O_3, SiO_2, CuO, ZnO and TiO_2. The research on nanofluid jet impingement has been carried out through experiments and numerical method in either a free-surface jet and a confined jet mostly to investigate the main parametric effects on heat transfer such as Reynolds number, jet-to-plate spacing and nanofluid concentration. Then, the correlations were presented. Zeitoun & Ali (2012), Modak et al. (2015) and Lv et al. (2017b) experimentally exhibited the heat transfer enhancement of the water-based Al_2O_3 nanofluid by approximately 60% at moderate concentration ($\phi \leq 6\%$ by volume) compared to the base fluid. Lv et al. (2017a) investigated the SiO_2 nanofluid impingement leading to the maximum 40% enhancement at Re = 8000 and ϕ = 3%. Barewar et al. (2019) studied Zuo nanofluid impingement at low concentration ($0.02 \leq \phi \leq 0.1\%$) and reported the maximum heat transfer augmentation by 55% at ϕ = 0.1% and H/D_j = 3.5. Naphon & Nakharintr (2012) used TiO_2 nanofluid at a fixed ϕ = 0.2% impinging on a mini fin heat sink to test the influence of the jet inlet temperature (T_j) and found that at higher T_j, i.e., 30°C the nanofluid did not help enhance the heat transfer. However, at lower T_j, i.e., 20°C the nanofluid became enhancing the heat transfer. The pressure drop data were also reported.

There have been a growing number of numerical analyses on the nanofluid impinging jet. Manca et al. (2011) investigated a slot jet of Al_2O_3 nanofluid using a single phase and k-ε turbulence model to study the effects of Reynolds number, jet-to-plate spacing (H/b) and concentration. They found the maximum heat transfer enhancement by 18% at ϕ = 6% and H/b = 10. Furthermore, they explained the decrease in heat transfer at the small H/b that was because the jet counter-rotating vortices were forced to leave before touching the stagnation region causing the secondary peak. Two-phase model for the Al_2O_3 nanofluid impingement was investigated by Huang & Jang (2013) and Abdelrehim et al. (2019). Abdelrehim et al. (2019) studied the laminar jet impingement and reported that the two-phase model gave better heat transfer results than the single-phase model when compared to the experimental ones. Alabdaly et al. (2019) numerically investigated a 2D planar laminar impinging jet of SiO_2 nanofluid on different sizes of semicircle bumps installed at some distance after the stagnation region. The higher Nusselt number was reported at the higher bump.

TiO_2 is nontoxic and inexpensive material used in variety of our everyday life including as a dye for off-white color in soap making process. However, not much research on nanofluid heat transfer include TiO_2 as nanoparticles, even though the heat transfer augmentation among TiO_2, Al_2O_3 and CuO nanofluids were found insignificantly different by Roy et al. (2012). Furthermore, few research work has reported pumping power or pressure drop (mostly carried out via numerical analysis research such as Abdelrehim et al. (2019), Alabdaly & Ahmed (2019), Roy et al. (2012) and Manca et al. (2011), but the experimental work by Naphon & Nakharintr (2012) showed the data of pressure drop) and the heat transfer correlations (carried out through either numerical investigation or experiments such as Lv et al, (2017a, b), Zeitoun & Ali (2012), Barewar et al. (2019), Modak et al. (2015) and Abdelrehim et al. (2019)) altogether, which are essential to heat transfer-related machine design.

The objectives of this research are to propose an alternative way of onsite cooling a CPU chip and to find the heat transfer characteristics of a circular impinging jet of water-based TiO_2 nanofluid on to a constant heat flux surface for both flat and chip surfaces. Parametric effects such as nanofluid concentration (ϕ), Reynolds number (Re) and jet-to-plate spacing (H/D_j) are considered. The heat transfer results are reported in terms of local and area average Nusselt numbers. With the use of the multiple linear regression, the heat transfer correlations are presented. Finally, pumping power ratios of the nanofluid and the base fluid are also discussed.

3. RESEARCH METHODOLOGY

Throughout this study, a steady state, incompressible single-phase turbulent flow is assumed. In addition, at the impingement surface, the constant heat flux is assigned with assumption of no heat radiation. The jet impingement system is semi-confined with no end effect assumption.

3.1 Computational Domain

Two schematic setups of the 2D axi-symmetric computational domains were tested in this study as shown in Fig 1. A circular jet nozzle of radius 2 mm is attached to a flat surface to form an upper boundary for the computational domain. A CPU chip of 9.15 mm radius (R_{chip}) and 5 mm height exhibited in Fig.1(a) is placed under the nozzle. The constant heat flux surface is

assigned to the chip surface only, and the rest of the impingement plate is insulated. In Fig.1(b), the entire flat plate is assigned constant heat flux. All surfaces within the domain are at no-slip condition with the radius (R_s) of 25 mm. After impinging, the spent fluid is to leave the exit, at which, the pressure is set to be equal to the ambient pressure.

Nanofluid of TiO_2 nanoparticles in water as a base fluid is the working fluid in this study. Pure water is also used for baseline cases. Hence, in this study, the heat transfer of the free-surface liquid jet impingement is considered.

3.2 Governing Equations

Under assumptions of steady state, incompressible, turbulent, single-phase flow and negligible heat radiation, The Reynolds time averaged Navier-Stokes (RANS) equations are shown in as follows

Continuity:

$$\frac{\partial \bar{u}_i}{\partial x_i} = 0 \tag{1}$$

Momentum:

$$\rho \bar{u}_i \frac{\partial \bar{u}_i}{\partial x_j} = -\frac{\partial \bar{p}}{\partial x_i} + \frac{\partial}{\partial x_j}\left[\mu\left(\frac{\partial \bar{u}_i}{\partial x_j} + \frac{\partial \bar{u}_j}{\partial x_i}\right) - \rho\overline{u_i' u_j'}\right] \tag{2}$$

Energy:

$$\rho \bar{u}_i \frac{\partial \bar{T}}{\partial x_j} = \frac{\partial}{\partial x_j}\left[\frac{\mu}{Pr}\frac{\partial \bar{T}}{\partial x_j} - \rho\overline{T' u_j'}\right] \tag{3}$$

where $\bar{u}_i$, $\bar{u}_j$, $\bar{T}$ and $\bar{p}$ are time-averaged velocity components, temperature and pressure, respectively.

u_i', u_j' and T' are fluctuating quantities.

Noting that the Reynolds stress term, $-\rho\overline{u_i' u_j'}$, is based upon the Boussineq hypothesis show as follows

$$-\rho\overline{u_i' u_j'} = \nu_t\left(\frac{\partial \bar{u}_i}{\partial x_j} + \frac{\partial \bar{u}_j}{\partial x_i}\right) - \frac{2}{3}\delta_{ij} \tag{4}$$

and the turbulent heat flux term

$$\rho\overline{T' u_j'} = \frac{\mu_t}{Pr_t}\left(\frac{\partial \bar{T}}{\partial x_j}\right) \tag{5}$$

The k-ε turbulence model with wall treatment for the steady state impinging jet with the assumption of fully developed turbulent flow is exhibited in the following equations. These equations combined with the above RANS equations thus govern the turbulent flow and heat transfer of the domain.

Energy:

$$\frac{\partial(\rho k u_i)}{\partial x_j} = \frac{\partial}{\partial x_j}\left(\mu + \frac{\mu_t}{\sigma_k}\right)\frac{\partial k}{\partial x_j} + (G_k + G_b) - \rho\varepsilon - Y_M + S_\varepsilon \tag{6}$$

Dissipation:

$$\frac{\partial(\rho\varepsilon u_i)}{\partial x_j} = \frac{\partial}{\partial x_j}\left(\mu + \frac{\mu_t}{\sigma_\varepsilon}\frac{\partial \varepsilon}{\partial x_j}\right) + C_1\frac{\varepsilon}{k}(G_k + G_{3\varepsilon}G_b) - C_2\rho\frac{\varepsilon^2}{k} + S_\varepsilon \tag{7}$$

where G_k and G_b denote the turbulent kinetic energy (tke) production terms due to the velocity gradients and the buoyancy, respectively. Y_M is the fluctuation rate associated with the tke dissipation. σ_k and σ_ε represent effective Prandtl numbers, which associates to eddy diffusion of k and ε to the momentum eddy viscosity as shown below

$$\sigma_k = \frac{\nu_t}{\nu_k} \quad \text{and} \quad \sigma_\varepsilon = \frac{\nu_t}{\nu_\varepsilon}$$

and the eddy viscosity is

$$\nu_t = \frac{C_\mu k^2}{\varepsilon}$$

The empirical constant values for jet impingement are C_μ = 0.09, C_1 = 1.44, C_2 = 1.92, σ_k = 1.0, and σ_ε = 1.3. The buoyancy dependence rate of ε is denoted $C_{3\varepsilon}$ which is equal to $\tanh|v/u|$. S_k and S_ε represent the generation terms.

3.3 Finite Element Method

A commercial program of finite element method, COMSOL, was used throughout the study. The program uses free meshing techniques to generate unstructured meshes covering the computational domain. Each mesh element is a triangle of 3 vertex node with linear shape function for all unknown variables: velocity components, pressure and temperature.

Note on the wall treatment with the use of k-ε turbulence model in COMSOL that the wall life-off from the physical surface was defined as $\delta_W = \frac{\delta_W^+ \mu}{\rho u_\tau}$, where the term δ_W^+ is determined from $\delta_W^+ = \max\left(\frac{h_w}{2}\frac{\rho C_\mu^{1/4}\sqrt{k}}{\mu}, 11.06\right)$ whether which one is higher. The first term is derived from the law of the wall, and the second one refers to the distance measured from the wall, where the logarithmic layer encounters with the laminar sublayer. Here h_w is denoted by the height of the mesh adjacent to the wall.

The boundary conditions shown in Fig.1. All surfaces are set no-slip conditions. The thermal boundary conditions at surfaces are set insulated or dT/dt = 0 except at the impingement surface, i.e., the entire plate for the flat plate case (Fig.1(a)) and the chip surface for the chip plate (Fig.1(b)). The inlet toward the impingement plate is at the nozzle exit. Finally, after impinging the fluid leaves the surface toward the exit to ambient.

3.4 Data Reduction

In this study, 3 parametric effects are considered: Reynolds number (Re_{Dj}), jet-to-plate spacing (H/D_j) and nanofluid concentration (ϕ), and the values are shown in

Table 1. The heat transfer results are expressed in terms of heat transfer coefficient (h) and Nusselt number (Nu_{Dj}). The results are presented as the dimensionless heat transfer correlations for both flat and chip surfaces.

Single phase fluid is assumed throughout the study. The nanoparticles of TiO_2 change the thermal properties of the base fluid, such as density (ρ), dynamic viscosity (μ), thermal conductivity (λ) and specific heat (c_p) according to the empirical formulae summarized by Said et al. (2014).

$$\rho_{nf} = (1-\phi)\rho_{bf} + \phi\rho_P \quad (8)$$

$$\mu_{nf} = \mu_{bf}(123\phi^2 + 7.3\phi + 1) \quad (9)$$

$$\lambda_{nf} = \lambda_{bf}\left(\frac{\lambda_P + 2\lambda_{bf} + 2(\lambda_P - \lambda_{bf})\phi}{\lambda_P + 2\lambda_{bf} - (\lambda_P - \lambda_{bf})\phi}\right) \quad (10)$$

$$c_{p,nf} = (1-\phi)c_{p,bf} + \phi c_{p,P} \quad (11)$$

The subscripts nf, bf and P denote nanofluid, base fluid and nanoparticle, respectively.

The Reynolds number is defined based on jet diameter (D_j) as follows

$$Re_{D_j} = \frac{\rho u_j D_j}{\mu} \quad (12)$$

After obtaining the surface temperature (T_s) from the computation, Newton's law of cooling gives

$$h = \frac{q_s''}{(T_s - T_j)} \quad (13)$$

where the surface heat flux is set to be 500 kW/m^2. This value was obtained from the specification of the CPU chip of Intel Core i7-920 (Kirsch (2008)). Then, the area-averaged heat transfer coefficient is calculated.

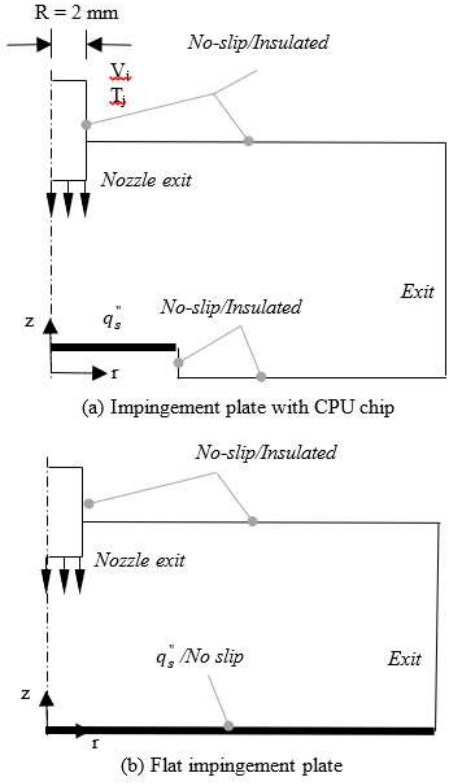

Figure 1 Computational domains and boundary conditions (Not to scale)

Table 1 Parametric effects and their values

Parametric effects	Values
Re_{Dj}	2000, 4000, 6000, 8000
H/D_j	2, 3, 4
ϕ (% Volume)	0, 2, 4, 6

3.5 Mesh Density Dependence Check

Four different models of number of meshes are tested as shown in Fig.2: 4800, 9480, 49628 and 100677 meshes, namely models A, B, C and D, respectively, in the flat impingement surface domain for Re = 2000, 4000, 6000 and 8000. The surface mesh sizes are mainly refined: 0.1, 0.05, 0.01 and 0.005 mm for models A, B, C and D, respectively. The results in terms of average Nusselt numbers are compared as well as computational time and RAM usage. Moreover, the mesh quality is also taken into consideration as the finer mesh costs lower quality, despite less error [Holzbecher & Si]. Model D is thus assumed to give the most accurate solution in terms of average Nusselt number.

The maximum difference from model D is found at model B for 7% at Re_{Dj} = 8000 while model A 6% at Re_{Dj} = 6000. However, when comparing models C and D, the difference is close to 0%. Considering RAM usage and computing times between models C and D, model C uses up to 0.5 GB less than model D while the computing time is nearly half of that of model D. The average mesh quality of model C is 11% higher. Therefore, model C is chosen to fit the accuracy and the specification of the computer used in this study is CPU Intel Corei5-8300H 4.0 GHz and 8 GB RAM.

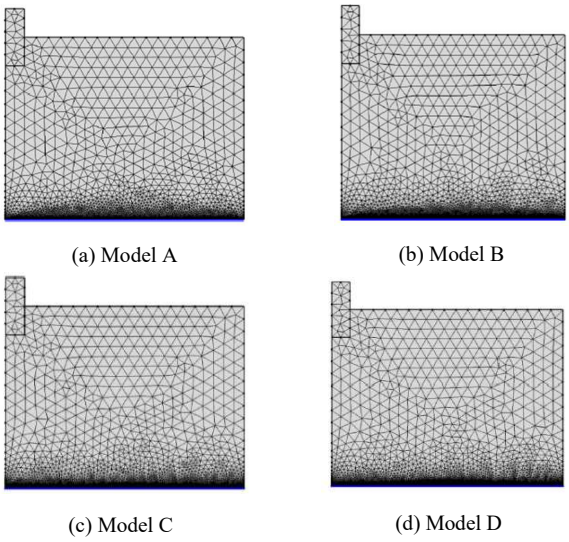

Figure 2 Mesh refinement especially near wall region

3.6 Validation

Fig.3 shows the comparison of the average Nusselt number obtained from the present study to the

experimental results of Sorour et al. (2019) at $H/D_j = 4$ and Re = 8000-14000. The differences are found 5.71%, 4.88%, 6.25% and 9.09% at 8000, 10000, 12000 and 14000, respectively. The differences were probably because the experimental setup of Sorour et al. (2019) was carried out through the heat flux of 14,920 W/m^2, D_j = 6 mm and D_s = 320 mm while the present computational domain was set to the heat flux of 500 kW/m^2, D_j = 4 mm and D_s = 50 mm. Sorour et al. (2019) showed that H/D_j did not significantly affect the Nusselt number.

The comparison of area averaged heat transfer coefficients of the current study to those of Lv et al. (2017) are shown in Fig.4. The tested Reynolds number in this study is from 2000 to 8000, while Lv at al. (2017) from 6114 to 12228, D_j = 2 mm, D_s = 100 mm, but the surface thermal condition was not reported. The similar trends of the data are found. Furthermore, both Lv et al. (2017) and the current study have also found that H/D_j slightly influences the heat transfer for the free-surface water impingement. However, for the clear illustration purpose, the heat transfer results for each H/D_j value are shown separately.

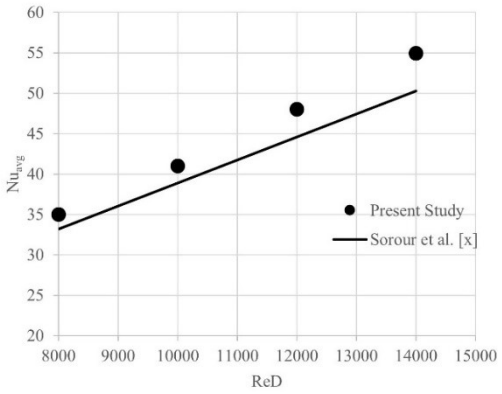

Figure 3 Comparison of the average Nusselt number of the present study and Sorour et al. (2019)

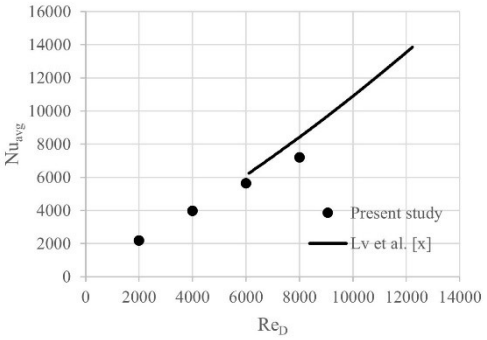

(a) $H/D_j = 2$

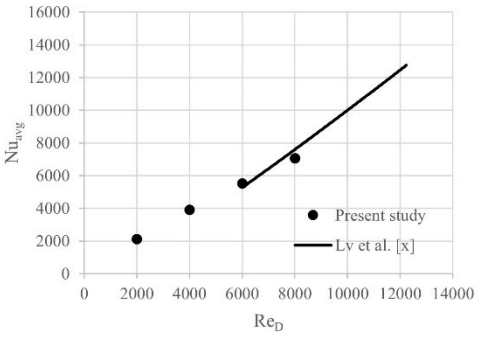

(b) $H/D_j = 3$

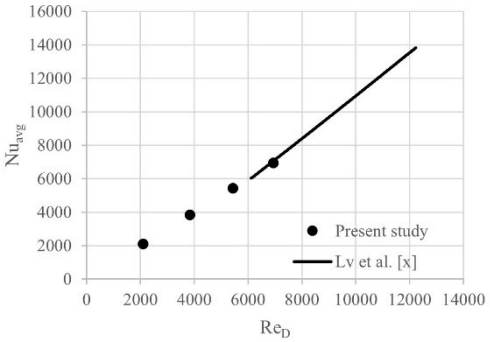

(c) $H/D_j = 4$

Figure 4 Comparison of heat transfer coefficients of the present study to those of Lv et al. (2017)

4. RESULTS AND DISCUSSION

4.1 Comparison of flow fields of flat plate impingement and chip plate impingement

Flat plate impingement as a baseline case is carried out along with the chip plate impingement in order to better understand the heat transfer results on the chip plate later on. Fig.5(a) shows the oncoming jet impinging on a flat surface and changing the flow direction along the impingement surface to form a wall jet then leave at the exit. In Fig.5(b), after impinging on a chip, the flow cannot leave towards the exit immediately, but circulates near the vicinity of the height of the chip prior to changing the direction along the flat area. This could be explained by the fact that the edge of the chip disrupts the boundary layer of the flow. Furthermore, according to Zhao et al. (2002), the chip surface covers the stagnation zone, while in Fig.5 (a) the viscous boundary layer starts right next to the stagnation zone. Note that the constant heat flux is assigned to the entire length of the flat plate case, while only to the chip surface and the flat area is insulated.

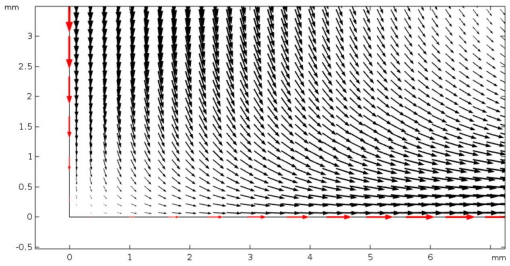

(a) Flat plate impingement

(b) Chip plate impingement

Figure 5 Vector plots of flow near the impingement vicinity

4.2 Effect of Nanofluid Concentration

Fig.6 shows the local Nusselt number distributions at Re = 8000 and H/D_j = 2 for different nanofluid concentrations. Note that only the chip surface is assigned constant heat flux and the heat transfer results on the chip surface are taken into account. Nusselt number increases with the nanofluid concentrations for both cases of flat plate and chip plate impingement. In Fig.6(a) for the flat plate impingement, the heat transfer enhancement of nanofluids compared to the base fluid at the stagnation point for Φ = 2, 4 and 6% are 3.38, 9.97 and 18.97%, respectively. However, the maximum value is shifted slightly away from the centerline and becomes the secondary peak for all cases. The differences in the secondary peak between the nanofluids of Φ = 2, 4 and 6% and the base fluid are 3.37, 9.96 and 18.97%, respectively. For the chip plate impingement, the differences in the stagnation points are 3.08, 9.80 and 18.89%, respectively. The differences in the secondary peaks are 9.08, 9.81 and 18.95%, respectively. According to Manca et al. (2011), the counter-rotating vortices of the oncoming jet towards the target plate are responsible for the secondary peaks as the vortices do not yet touch the stagnation point but are pushed away parallel to the surface towards the exit.

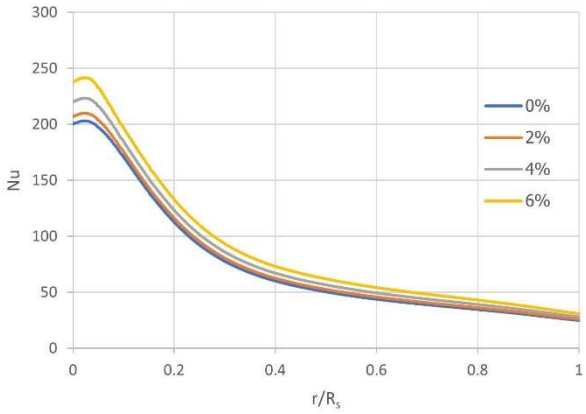

(a) Flat Plate

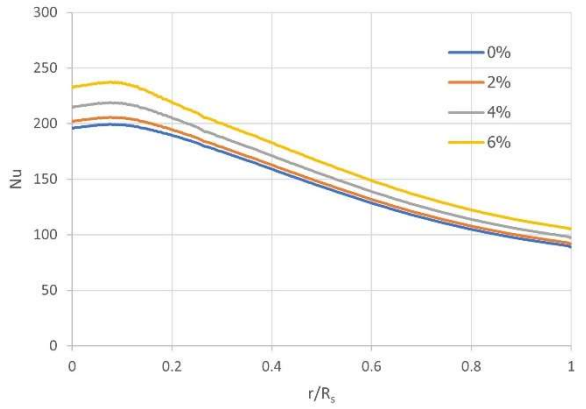

(b) Chip Plate

Figure 6 Local Nusselt number for different concentrations of Nanofluids at Re = 8000 and H/D_j = 2

However, the flow characteristics of nanofluids are not different from that of the base fluid (water), because the assumption of single phase nanofluid only changes the numeric values of the thermal properties of the working fluid. Nonetheless, Lv et al. (2017) confirmed with their experimental results that addition of the nanoparticles into a base fluid did not affect the flow characteristic of the base fluid explained by the individual nanoparticle bombardment effect on the surface. Thus, this helps enhance the heat transfer of the base fluid.

Fig.6(a) shows the comparison of area averaged Nusselt numbers at different concentrations for both flat

plate and chip plate impingement. The results are in accordance with the local Nusselt number variation that the heat transfer enhancement increases with the nanofluid concentration. The chip plate impingement gives higher average Nu than the flat plate due to the fact that only the chip surface was considered in the calculation, while the entire surface of flat plate impingement was brought into the calculation. The maximum heat transfer enhancement in terms of Nu_{avg} is 24.57% found at Re_{Dj} = 2000 and ϕ = 6% for the flat plate impingement and 18.24% at Re_{Dj} = 2000 and ϕ = 6% for the chip plate impingement. However, when considering in terms of area average heat transfer coefficients as exhibited in Figs.6(b) and (c) for the flat and the chip impingement, respectively, the maximum enhancement is also found at Re_{Dj} = 2000 and ϕ = 6% by 47.13% and 39.65%. Nevertheless, noting that the enhancement found at other values of Re_{Dj} (ϕ = 6%) is only 1-2% lower than at Re_{Dj} = 2000.

4.3 Effect of Reynolds Number

Generally, the impingement heat transfer results are significantly influenced by Reynolds number. Higher Re leads to higher heat transfer results as illustrated in Fig.7 for both flat and chip plate impingement as the jet velocity at the higher Re_{Dj} becomes higher and impinges more vigorously causing the boundary layer thinner. This also allows the jet with higher Re_{Dj} to exchange more momentum leading to higher heat transfer enhancement. The area average Nusselt numbers are plotted against Re_{Dj} at different values of jet-to-plate spacing, which will be discussed in the following topic. Re_{Dj} = 8000 gives the highest followed by Re_{Dj} = 6000, 4000 and 2000, respectively.

The area averaged Nusselt numbers at different Re and H/D_j are plotted in Fig.8 for ϕ = 4%. Consider Fig.8(a), H/D_j does not play important role to Nu_{avg} values. Re_{Dj} = 8000 gives the area average Nu approximately 70% higher than Re = 2000, and 44% and 21 higher than Re_{Dj} = 4000 and 6000, respectively, at all values of H/D_j. In Fig.8(b), the chip plate impingement shows the influence of H/D_j; however, the differences are similar. At Re_{Dj} = 8000, Nu_{avg} is approximately 64%, 39% and 18% higher than those at Re_{Dj} = 2000, 4000 and 6000, respectively.

4.4 Effect of Jet-to-Plate Spacing

Fig.10 shows the distribution of local Nusselt number for different jet-to-plate spacings at Re_{Dj} = 6000 and ϕ = 4%. Secondary peaks are found in all cases and prominently shown in the case of H/D_j = 2. This has been explained by some researchers (Cornaro et al. (1999), Manca et al.(2011) and Lv et al. (2017)) by the fact that at low H/D_j a jet cannot establish fully developed flow before approaching the target plate, thus the counter-rotating vortices are pushed parallel to the impingement surface towards the exit. Notwithstanding that, H/D_j = 2 leads to the highest local heat transfer results compared to H/D_j = 3 and 4.

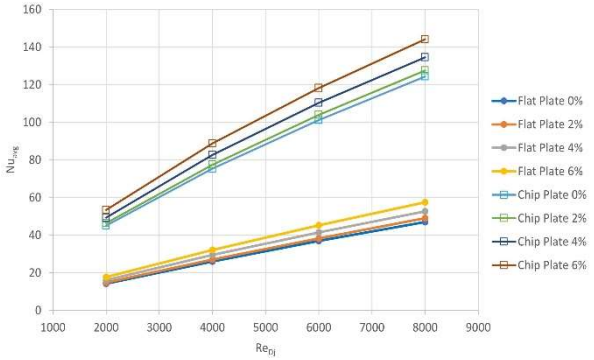

(a) Average Nusselt number

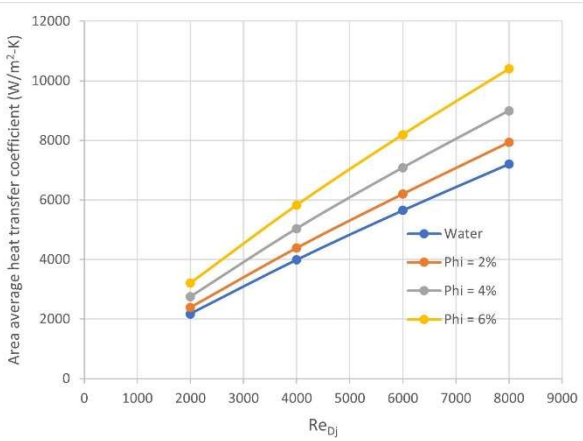

(b) Area average heat transfer coefficient for flat plate impingement

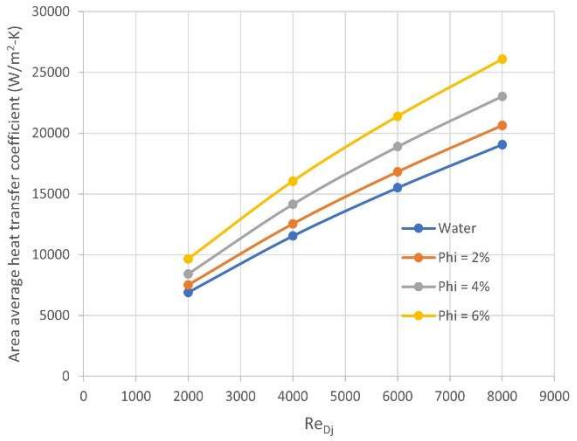

(c) Area average heat transfer coefficient for chip plate impingement

Figure 7 Average heat transfer results at H/D_j = 2.

Referring to the area averaged Nusselt numbers in Fig.9, H/D_j does not significantly affect the area average Nusselt number. This can be shown in the local distribution in Fig.10(a) that the local Nu graphs collapse after the stagnation zone. The area averaged Nu for the chip plate impingement is higher than the flat plate

impingement, because only the chip surface is included in the area average. The differences in percentage at each Re_{Dj} are quite similar such as at $H/D_j = 2$, Nu_{avg} is approximately 9% and 18% higher than those at $H/D_j = 3$ and 4, respectively, while at $H/D_j = 3$, Nu_{avg} is approximately 8% higher than that of $H/D_j = 4$.

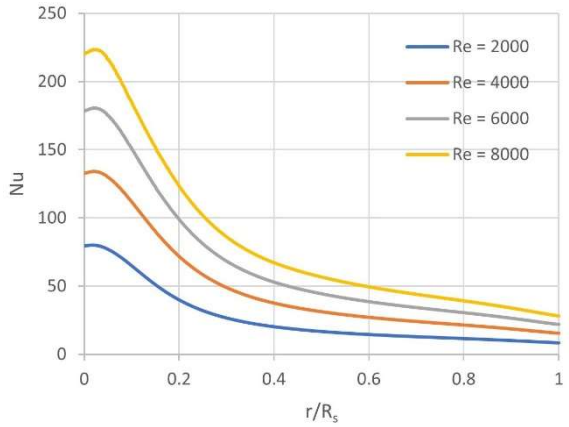

(a) Flat Plate

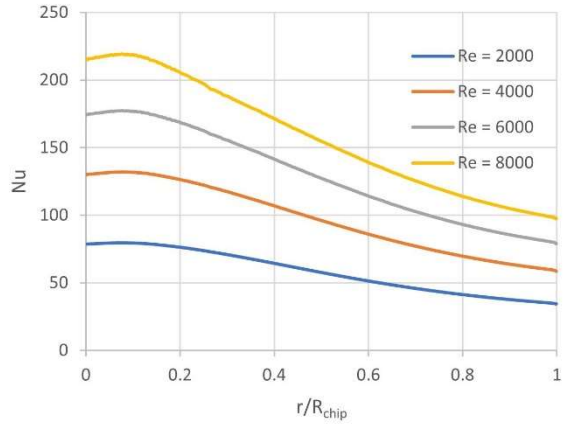

(b) Chip Plate

Figure 8 Comparison of local Nusselt number at different Reynolds number at $\Phi = 4\%$ and $H/D_i = 2$.

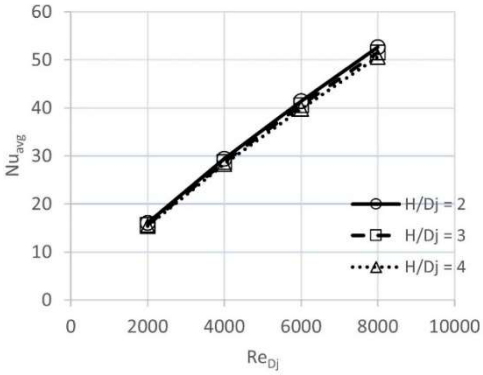

(a) Flat Plate

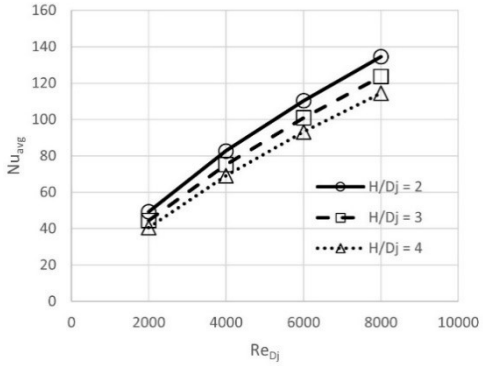

(b) Chip Plate

Figure 9 Comparison of area averaged Nusselt numbers for $\phi = 4\%$.

4.5 Heat Transfer Correlations

Nondimensional heat transfer correlations were obtained from the multiple linear regression analysis through the analysis of variance (ANOVA). The area averaged Nusselt number becomes the dependent variable or the response variable, and the independent variables or explanatory variables are Re_{Dj}, H/D_j and Φ. Then, all variables are log-transformed, then the multiple linear regression is performed with the R^2 value greater than 0.99 for all cases. In addition, 2-sided p-values for testing the coefficients are less than 0.05. Finally, after anti-logging, 4 heat transfer correlations are obtained: water impinging on a flat plate, nanofluid impinging on a flat plate, water impinging on a chip plate and nanofluid impinging on a chip plate.

For flat plate impingement, the correlation of Nusselt number to Reynolds number and jet-to-plate spacing is shown as follows

$$Nu_{avg} = 0.0209 Re_{D_j}^{0.8638} \left(H/D_j\right)^{-0.0557} \quad (16)$$

For the nanofluid impingement on a flat plate, the correlation is

$$Nu_{avg} = 0.0557 Re_{D_j}^{0.8587} \left(H/D_j\right)^{-0.056} \phi^{0.1458} \quad (17)$$

For impinging on the chip surface, only the heat transfer of the chip top surface was considered. In the case of water jet, the correlation is then

$$Nu_{avg} = 0.1922 Re_{D_j}^{0.7414} \left(H/D_j\right)^{-0.2622} \quad (18)$$

Finally, in the case of the nanofluid jet impinging on a chip, the correlation becomes

$$Nu_{avg} = 0.3247 Re_{D_j}^{0.7368} \left(H/D_j\right)^{-0.2522} \phi^{0.1206} \quad (19)$$

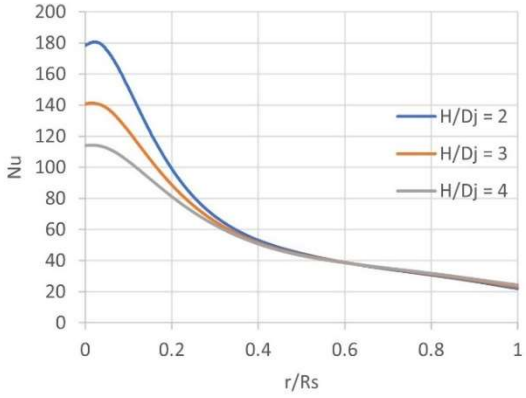

(a) Flat Plate

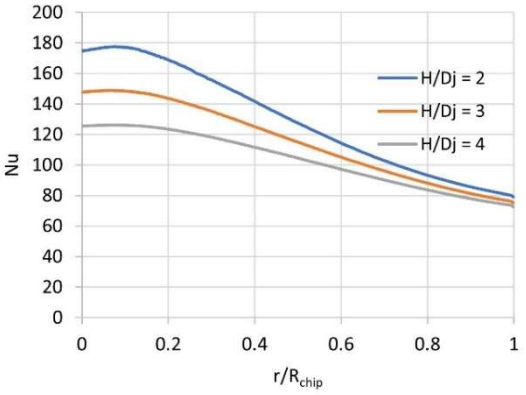

(b) Chip Plate

Figure 10 Distribution of local Nusselt numbers at different jet-to-plate spacing, Re_{Dj} = 6000, Φ = 4%

4.6 Pumping Power

Fig.11 shows the plots of pumping power ratio between the pumping power of nanofluid (PP_{nf}) and the pumping power of base fluid (PP_{bf}) against Reynolds number at H/D_j = 2. Since nanoparticles cause the viscosity of the base fluid to increase, the pumping power of the nanofluid is obviously higher than that of the base fluid. When ϕ = 2%, the pumping power becomes almost 50% higher than that of the base fluid at all values of Re_{Dj}. The pumping power is increased to be more than twice and almost 4 times of the base fluid, when the concentrations are increased to 4% and 6%, respectively. Therefore, the proper selection of the nanofluid concentration is important for nanofluid jet impingement, especially for experiments.

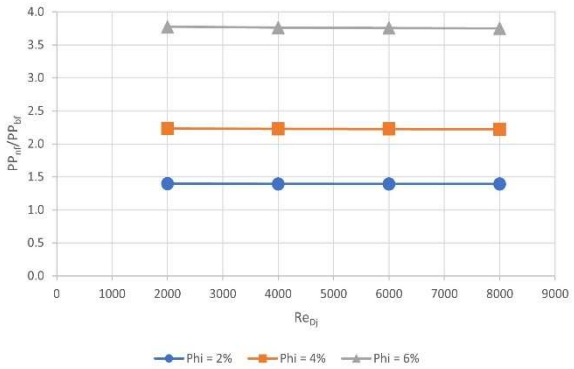

Figure 11 Pumping power ratios of nanofluid and water for chip plate impingement at H/D_j = 2

5. CONCLUSIONS

A numerical heat transfer study on water-based TiO_2 nanofluid impingement on a chip surface and on a flat surface was carried out to investigate the parametric effects such as nanofluid concentration, Reynolds number and jet-to-plate spacing as follows

1. The heat transfer increased with the increasing concentration due to the increasing in thermal conductivity. The maximum heat transfer enhancement in terms of Nusselt number was 24.57% and 18.24% for the flat plate and the chip plate impingement cases, respectively, at ϕ = 6% and Re_{Dj} = 2000.
2. As Reynolds number increased, the heat transfer also increased. This was explained by the fact that at higher Reynolds number the impinging jet thinned the boundary layer and allowed the greater momentum transfer.
3. Due to the counter-rotating vortices being pushed (according to Cornaro et al. (1999) and Manca et al. (2011)), the secondary peaks at the stagnation region were shown at all H/D_j cases. The heat transfer increased with decreasing H/D_j. However, the local Nu distribution showed that the local Nu collapsed after impingement region.

The heat transfer correlations for cases of both flat plate and chip plate impingement for the water and the nanofluid were presented by using the multiple linear regression analysis of log-log scale. After anti-logging, each correlation is summarized as follows

Water-flat plate impingement:

$$Nu_{avg} = 0.0209 Re_{D_j}^{0.8638} \left(H/D_j\right)^{-0.0557}$$

Nanofluid-flat plate impingement:

$$Nu_{avg} = 0.0557 Re_{D_j}^{0.8587} \left(H/D_j\right)^{-0.056} \phi^{0.1458}$$

Water-chip plate impingement:

$$Nu_{avg} = 0.1922 Re_{D_j}^{0.7414} \left(H/D_j\right)^{-0.2622}$$

Nanofluid-flat plate impingement:

$$Nu_{avg} = 0.3247 Re_{D_j}^{0.7368} \left(H/D_j\right)^{-0.2522} \phi^{0.1206}$$

Even though the nanofluid jet impingement has shown a promising heat transfer enhancement, the

penalty in pressure drop in terms of pumping power was also considered. At ϕ = 6%, the pumping power was found almost 4 times of that of water, while at ϕ = 2% the pumping power became 50% of that of water. These data are crucial for heat transfer component designers.

6. REFERENCES

Abdelrehim, O., Khater, A., Mohamad, A.A. & Radwan, A. (2019). Two-phase simulation of nanofluid in a confined single impinging jet. *Case Studies in Thermal Engineering*, 14, 100423. https://doi.org/10.1016/j.csite.2019.100423

Alabdaly, I.K. & Ahmed, M.A. (2019). Numerical investigation on the heat transfer enhancement using a confined slot impinging jet with nanofluid. *Propulsion and Power Research*, 8(4), 351-361. https://doi.org/10.1016/j.jppr.2019.06.004

Barewar, S.D., Tawri, S. & Chougule, S.S. (2019). Heat transfer characteristics of free nanofluid impinging jet on flat surface with different jet to plate distance: An experimental investigation. *Chemical Engineering & Processing: Process Intensification*, 136, 1–10. https://doi.org/10.1016/j.cep.2018.12.001

Choi, S.U.S. & Eastman, J.A. (1995). Enhancing thermal conductivity of fluids with nanoparticles. *ASME International Mechanical Engineering Congress & Exposition, November, 12-17, 1995, San Francisco, CA, USA.* https://www.osti.gov/biblio/196525-enhancing-thermal-conductivity-fluids-nanoparticles

Cornaro, C., Fleischer, A.S. & Goldstein, R.J. (1999). Flow visualization of a round jet impinging on cylindrical surfaces. *Experimental Thermal and Fluid Science*, 20(2), 66-78. https://doi.org/10.1016/S0894-1777(99)00032-1

Huang, J.B. & Jang, J.Y. (2013). Numerical Study of a Confined Axisymmetric Jet Impingement Heat Transfer with Nanofluids. *Engineering*, 5, 69-74. doi:10.4236/eng.2013.51b013

Holzbecher, E., & Hand, S. (2008). Accuracy test for COMSOL – and Delaunay meshes. COMSOL. *Excerpt from the Proceedings of the COMSOL Conference 2008 Hannover.* https://www.comsol.com/paper/accuracy-tests-for-comsol-and-delaunay-meshes-5436

Kirsch, N. (2008, Nov 03). Intel Core i7 920, 940 and 965 Processor Review. Retrieved from http://www.legitreviews.com/intel-core-i7-920-940-and-965-processor-review_824#vkxPL2aZHwzDJ1zl.99

[a]Lv, J., Chang, S., Hu, C., Bai, M., Wang, P. & Zeng, K. (2017). Experimental investigation of free single jet impingement using Al_2O_3-water nanofluid. *International Communications in Heat and Mass Transfer*, 88, 126–135. http://dx.doi.org/10.1016/j.icheatmasstransfer.2017.08.017

[b]Lv, J., Hu, C., Bai, M., Zeng, K, Chang, S. & Gao, D. (2017). Experimental investigation of free single jet impingement using SiO_2-water nanofluid. *Experimental Thermal & Fluid Science, 84*, 39-46. http://dx.doi.org/10.1016/j.expthermflusci.2017.01.010

Manca, O., Mesollela, P., Nardini, S. & Ricci, D. (2011). Numerical study of a confined slot impinging jet with nanofluids. *Nanoscale Research Letters,* 6, 188. http://www.nanoscalereslett.com/content/6/1/188

Modak, M., Srinivasan, S., Garg, K., Chougule, S.S., Agarwal, M.K. & Sahu, S.K. (2015). Experimental investigation of heat transfer characteristics of the surface using Al_2O_3–water nanofluids. *Chemical Engineering & Processing: Process Intensification*, 91, 104–113. http://dx.doi.org/10.1016/j.cep.2015.03.006

Naphon, P. & Nakharintr, L. (2012). Nanofluid jet impingement heat transfer characteristics in the rectangular mini-fin heat sink. *Journal of Engineering Physics and Thermophysics*, 85(6). https://link.springer.com/article/10.1007/s10891-012-0793-8

Roy, G., Gherasim, I., Nadeau, F., Poitras, G. & Nguyen, C.T. (2012). Heat transfer performance and hydrodynamic behavior of turbulent nanofluid radial flows. International Journal of Thermal Sciences 58, 120-129. doi:10.1016/j.ijthermalsci.2012.03.009

Said, Z., Saidur, R., Hepbasli, A. & Rahim, N.A. (2014). New thermophysical properties of water based TiO_2 nanofluid – the hysteresis phenomenon revisited. *International Communications in Heat and Mass Transfer*, 58, 85-95. http://dx.doi.org/10.1016/j.icheatmasstransfer.2014.08.034

Sorour, M.M., El-Maghlany, W.M., Alnakeeb, M.A. & Abbass, A.M. (2019). Experimental study of free single jet impingement utilizing high concentration SiO_2 nanoparticles water base nanofluid. *Applied Thermal Engineering*, *160*, 114019. https://doi.org/10.1016/j.applthermaleng.2019.114019

van Erp, R., Soleimanzadeh, R., Nela, L, Kampitsis, K. & Matioli, E. (2020). Co-designing electronics with microfluidics for more sustainable cooling. *Nature, 585*, 211-216. https://www.nature.com/articles/s41586-020-2666-1

Wei, T., Oprins, H., Cherman, V., Qian, J., Wolf, I.D., Beyne, E.& Baelmans, M. (2019). High-efficiency polymer-based direct multi-jet impingement cooling solution for high-power devices. *IEEE Transaction on Power Electronics*, 34(7), 6601-6612.

Zeitoun, O. & Ali, M. (2012). Nanofluid impingement jet heat transfer. *Nanoscale Research Letters*, 7:139. http://www.nanoscalereslett.com/content/7/1/139

Zhao, Y., Masuoka, T., Tsuruta, T. & Ma, C.F. (2002) Conjugate heat transfer on a horizontal surface impinged by circular free-surface liquid jet. *JSME International Journal series B,* 45(2), 307-314. https://doi.org/10.1299/jsmeb.45.307